ARMY RESEARCH LABORATORY

# Simulated Radar Range Profiles of a Simple Room as Computed by FDTD and Xpatch

by Traian Dogaru and Calvin Le

**ARL-TR-4420**                                                  **April 2008**

**NOTICES**

**Disclaimers**

The findings in this report are not to be construed as an official Department of the Army position unless so designated by other authorized documents.

Citation of manufacturer's or trade names does not constitute an official endorsement or approval of the use thereof.

Destroy this report when it is no longer needed.  Do not return it to the originator.

# Army Research Laboratory

Adelphi, MD 20783-1197

# Simulated Radar Range Profiles of a Simple Room as Computed by FDTD and Xpatch

**Traian Dogaru and Calvin Le**
**Sensors and Electron Devices Directorate, ARL**

| REPORT DOCUMENTATION PAGE | | | *Form Approved* *OMB No. 0704-0188* | |
|---|---|---|---|---|

Public reporting burden for this collection of information is estimated to average 1 hour per response, including the time for reviewing instructions, searching existing data sources, gathering and maintaining the data needed, and completing and reviewing the collection information.  Send comments regarding this burden estimate or any other aspect of this collection of information, including suggestions for reducing the burden, to Department of Defense, Washington Headquarters Services, Directorate for Information Operations and Reports (0704-0188), 1215 Jefferson Davis Highway, Suite 1204, Arlington, VA 22202-4302. Respondents should be aware that notwithstanding any other provision of law, no person shall be subject to any penalty for failing to comply with a collection of information if it does not display a currently valid OMB control number.
**PLEASE DO NOT RETURN YOUR FORM TO THE ABOVE ADDRESS.**

| 1. REPORT DATE *(DD-MM-YYYY)* | 2. REPORT TYPE | 3. DATES COVERED (From - To) |
|---|---|---|
| April 2008 | Final | 2007 to 2008 |

| 4. TITLE AND SUBTITLE | 5a. CONTRACT NUMBER |
|---|---|
| Simulated Radar Range Profiles of a Simple Room as Computed by FDTD and Xpatch | |
| | 5b. GRANT NUMBER |
| | 5c. PROGRAM ELEMENT NUMBER |
| **6. AUTHOR(S)** | 5d. PROJECT NUMBER |
| Traian Dogaru and Calvin Le | |
| | 5e. TASK NUMBER |
| | 5f. WORK UNIT NUMBER |

| 7. PERFORMING ORGANIZATION NAME(S) AND ADDRESS(ES) | 8. PERFORMING ORGANIZATION REPORT NUMBER |
|---|---|
| U.S. Army Research Laboratory<br>ATTN: AMSRD ARL SE RU<br>2800 Powder Mill Road<br>Adelphi, MD 20783-1197 | ARL-TR-4420 |

| 9. SPONSORING/MONITORING AGENCY NAME(S) AND ADDRESS(ES) | 10. SPONSOR/MONITOR'S ACRONYM(S) |
|---|---|
| | 11. SPONSOR/MONITOR'S REPORT NUMBER(S) |

**12. DISTRIBUTION/AVAILABILITY STATEMENT**

Approved for public release; distribution unlimited.

**13. SUPPLEMENTARY NOTES**

**14. ABSTRACT**

This technical report presents numerical simulations of the ultra-wideband (UWB) radar return from a simple room with a human inside, with application to sensing through the wall (STTW) radar scenarios. We use the Finite Difference Time Domain (FDTD) and Xpatch modeling techniques to compute the range profiles of the room at specific incidence and observation angles. Our goal is to analyze the electromagnetic phenomenology in operating an UWB radar for STTW applications. At the same time, we are interested in understanding issues specific to these computational techniques as applied to this type of problems, as well as validating Xpatch as an accurate tool for modeling general STTW radar scenarios.

**15. SUBJECT TERMS**

Sensing through the wall, radar, computational electromagnetics

| 16. SECURITY CLASSIFICATION OF: | | | 17. LIMITATION OF ABSTRACT | 18. NUMBER OF PAGES | 19a. NAME OF RESPONSIBLE PERSON<br>Traian Dogaru |
|---|---|---|---|---|---|
| a. REPORT | b. ABSTRACT | c. THIS PAGE | SAR | 40 | 19b. TELEPHONE NUMBER *(Include area code)* |
| U | U | U | | | 301-394-1482 |

**Standard Form 298 (Rev. 8/98)**
**Prescribed by ANSI Std. Z39.18**

# Contents

# List of Figures

v

# Acknowledgments

# 1. Introduction

Through-the-wall sensing is currently a topic of great interest to defense agencies both in the U.S. and abroad. Among the large spectrum of sensors that have been considered, low-frequency ultra-wideband (UWB) radar offers great potential for detecting targets behind walls, as well as for building imaging. The major challenge for this type of scenario, which involves the penetration of electromagnetic waves through a lossy medium concealing the target, is the trade-off between good penetration properties and good resolution, while trying to maintain a realistic antenna size/power requirement. Operating the radar in the low frequency microwave range (500 MHz to 3 GHz) has the advantage of good penetration through building structures.

Although the UWB radar technology has been considered in the context of sensing through the wall (STTW) applications for a few years now (*1 through 3*), there are still many less-understood aspects that require investigation. Among them we can list: the radar signature of the human body, the Doppler signature of a moving human, the transmission properties of walls (and, related, the electric properties of construction materials), synthetic aperture radar (SAR) techniques for building imaging, signal and image processing techniques that exploit the radar-collected information, as well as hardware issues involved in designing and building a STTW radar system. The U.S. Army Research Laboratory (ARL) has been active in all these fields of investigation, approaching these issues both through hardware design and radar measurements and through computer simulation of various STTW scenarios. We are currently involved in two major STTW programs within the Department of Defense (DoD), as well as participating in international panels on STTW technologies with military applications.

In a previous study (*4*), we investigated the radar signature of the human body in free-space from a computer modeling perspective. Continuing our research in computer modeling for STTW radar applications, this present report tackles larger-scale simulations, where we place the human body in a simple room. In this report, we focus on the radar return from the room at a single observation angle, by computing the range profiles resulting from a short pulse excitation. For this purpose, we use two modeling techniques for radar signature computation, namely the Finite-Difference Time-Domain (FDTD) and Xpatch.

The propagation of electromagnetic waves through buildings has received a great amount of interest in connection with the wireless communication devices, which have become omnipresent nowadays. Computer modeling of such phenomena usually involve techniques such as ray tracing, physical optic (PO), geometric theory of diffraction (GTD) and other related field computation methods (*5 through 7*). All these are approximate techniques, which work accurately when the scattering structures are much larger than the wavelength. Exact field computation methods, such as FDTD, have also been applied to this type of problems, but only for two-dimensional problems (*8 through 11*), or hybridized with some approximate, high-

1

frequency technique (*12,13*).  More recently, FDTD was used in full three-dimensional simulations of wave propagation within building structures, for near-field sources and receivers (*14,15*).  The present study is the first reported attempt to model three-dimensional far-field radar scattering from room structures entirely by FDTD.  The major challenge in our approach is the large size of the computational space, which extends tens of wavelengths across in all directions.  Therefore, we start by analyzing the issues related to this type of simulation and finding solutions to eliminate eventual modeling artifacts.  For the Xpatch models we are confronted with a completely different type of challenge.  Although Xpatch is a very efficient code, capable of solving large problems (in an electromagnetic sense) with a modest amount of computational resources, its accuracy at relatively low microwave frequencies (such as the bands used by typical STTW radars) has not been sufficiently investigated.  Consequently, one major task of our study is to validate the Xpatch models for STTW radar applications and establish its limitations in simulating such scenarios.  We achieve this by comparing the Xpatch and FDTD radar signatures of the same room.

Besides understanding the issues involved in applying certain computational electromagnetic (CEM) codes to model basic STTW radar problems, our purpose is to investigate the phenomenology involved in operating a STTW UWB radar.  Based on these computer models, we are able to make recommendations to radar system designers with regard to essential parameters, such as frequency of operation, bandwidth, aperture size, polarization etc.

This report is organized as follows.  First, we present a short overview of the modeling methods used in this study (section 2).  The modeling results are presented in section 3.  We introduce the computational meshes and radar parameters in section 3.1 then analyze the FDTD results for basic configurations in section 3.2.  The Xpatch results are compared to FDTD in sections 3.3 through 3.5, for various scenarios.  In section 3.6 we explore the idea of operating the radar in cross-polarization mode.  We finalize with conclusions in section 4.

## 2.  Overview of the Electromagnetic Modeling Techniques

As mentioned in the Introduction, for this study we employ two widely used CEM modeling techniques, namely FDTD and ray-tracing combined with PO.  The FDTD code we used for this work is called AFDTD and was entirely developed at ARL for radar signature modeling.  We also used Xpatch, which is a ray-tracing-based code, developed by Science Applications International Corporation (SAIC) under a grant from the U.S. Air Force.  Since we made a detailed presentation of these codes in some previous reports (*4,16*), we will confine this section to a very brief introduction.  Also, the reader interested in finding more information is directed to a number of books and references to these subjects (*17 through 19*).

The FDTD algorithm is based on discretizing Maxwell's time-domain equations, using finite differences in spatial and temporal dimensions. The computational space, with a uniform, rectangular, grid-like structure, is made of elementary cubic cells. The electromagnetic field components are computed along the cell's edges and faces, at discrete time steps. By discretizing Maxwell's equations in time and space, we obtain the so-called FDTD update equations, which allow updating of a current field component sample, based on the values of neighboring field component samples obtained at a previous time step. The main advantages of the FDTD algorithm are the simplicity of implementation, the efficiency of parallelization, the fact that it can handle almost arbitrary media electric properties and geometries and can also provide results over a wide range of frequencies in one time-marching run. The major disadvantage of the FDTD technique is its computational cost, which scales up very rapidly with the physical size of the computational domain and the frequency of interest. Consequently, although FDTD is an exact solver capable of simulating a wide range of radar scenarios, there are certain bounds to the problem size that can be solved in a reasonable amount time with limited computer resources.

Xpatch is part of a family of CEM techniques that rely on high-frequency approximations to model field propagation and scattering. In particular, it implements ray tracing combined with PO (*20*) to compute the radar return from arbitrary targets. The code has a powerful built-in graphics user interface (GUI), which allows the user to draw and analyze complex meshes, and visualize the data. In the applications presented here, the meshes describe the target surface, using a triangular facet model. Although Xpatch has been successfully used in a large number of radar applications, it has a number of limitations, which stem from the approximate nature of the methods it implements. Thus, the PO approximation may produce wrong results at angles off the specular direction, and cannot accurately account for diffraction from dielectric wedges. Also, it does not capture important wave phenomena, such as surface, creeping, or traveling waves, as well as some interesting effects in multiple scattering scenarios. However, as compared to FDTD, Xpatch can achieve vastly superior speed in modeling radar problems (typically 100 to 1000 times faster).

We have performed the simulations in this study at the U.S. Army Major Shared Resource Center (MSRC) (*21*) on Linux Networx Evolocity II clusters. Note that the room modeling is the largest production run to date where we have used the AFDTD software. We employed the parallel version of this code, run on 24 processors for each different case or angle of incidence. All the graphics in this report were done with Pioneer RCS. The pre- and post-processing were performed on Dell workstations running Windows XP.

# 3.   Numerical Results

## 3.1.   Computational Meshes and Radar Parameters

The geometry of the room we analyzed in this study is shown in figure 1.  The room dimensions are 5 m x 3.5 m x 2.2 m, with the radar looking usually perpendicular to the widest side (which represents the $\phi = 0°$ azimuth direction).  The human is placed in the middle of the room.  In the first part of our study, we investigate a ground-based radar scenario, where the elevation angle is 0° (propagation vector in the *x-y* plane).  For this case, the entire room is placed in free-space, meaning there is no infinite ground plane underneath the walls (a plane wave propagating at 0° elevation in the presence of an infinite ground plane would produce null total fields everywhere in the space).  However, in most cases, we add a flat ceiling and a floor with the exact same extent as the room perimeter (those cases will be explained in the next section).  In figure 1 these appear in yellow.  The FDTD grids have a resolution (cubic cell size) of 5 mm, and their overall size is on the order of 780 x 1020 x 500 cells.  For Xpatch, the walls are created by triangular facets in a very simple manner: each rectangle is made up of two triangles.  More complex in this case is the human mesh, which contains approximately 35,000 facets with an average edge size of 1 cm.



Figure 1.  Geometry of the room used in calculating the radar range profiles
in sections 3.1 through 3.4; the exterior dimensions are
5 m by 3.5 m by 2.2 m, with 8 in. thick walls and 6 in. thick concrete
slabs covering the bottom and the top; the fit man is placed in the
middle of the room.

We looked at three different construction materials for the walls: brick, concrete and cinder blocks. All walls are 8" thick. The brick walls are made of a uniform dielectric with $\varepsilon_r = 3.8$, $\sigma = 0.03$ S/m (for FDTD) or $\varepsilon' = 3.8$, $\varepsilon'' = 0.24$ (for Xpatch) (*22 through 25*). The difference between the two models was dictated by constraints built into the CEM codes. We tried to minimize the impact of this issue on the radar range profiles by matching the conductivity and the imaginary part of the permittivity in the middle of the frequency band. In both cases the building material is concrete, with $\varepsilon_r = 6.8$, $\sigma = 0.1$ S/m (for FDTD) or $\varepsilon' = 6.8$, $\varepsilon'' = 0.9$ (for Xpatch) (*22 through 25*). Whereas for the solid concrete walls the dielectric material is uniform, the cinder blocks exhibit internal air gaps. A schematic representation of a cinder block is shown in figure 2a, whereas a top view of the entire mesh (ceiling and floor removed) is shown in figure 2b. Note that, when the cinder blocks are properly aligned, they form "air tubes" that run continuously along the wall height. The ceiling and floor are always represented as 6" thick concrete slabs. Since the wall geometry is relatively simple, it was generated directly by the Xpatch GUI (as a triangular facet model), and then converted by an ARL-developed mesh converter program (AFDTDGRID) to an FDTD grid.
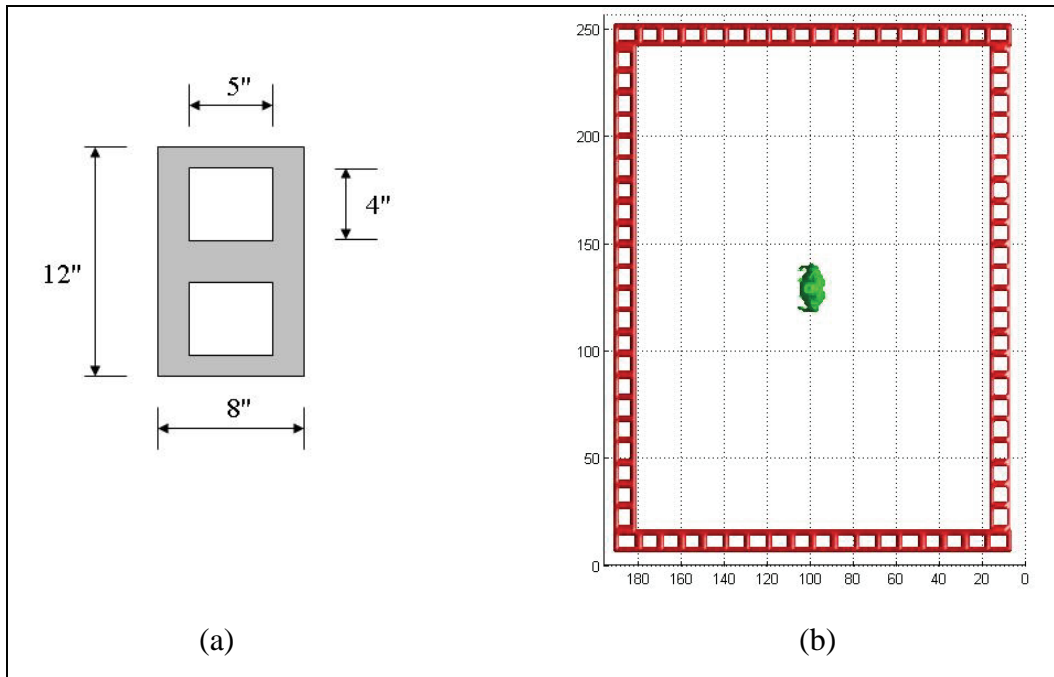


Figure 2. (a) Detailed view of a cinder block. (b) Top view of the room with cinder block walls.

The human mesh represents the "fit man", as described in (*4*). We obtained this body mesh from a commercial Web site (*26*). Since this model does not include the internal structure of the body, but only the exterior shell, we must assume that the entire body is made of the same uniform dielectric material. We picked for this material dielectric properties close to those of skin ($\varepsilon_r = 50$, $\sigma = 1$ S/m for FDTD or $\varepsilon' = 50$, $\varepsilon'' = 12$ for Xpatch). The validity of this uniform dielectric model for the human body was discussed in (*4*).

5

We assume that the radar operates as an UWB pulsed radar, and we are interested in analyzing the backscatter return corresponding to only one transmitted pulse, at a specific set of incidence angles. Since both modeling methods operate with plane waves in the far field, the antenna pattern is irrelevant to this scenario. Therefore, we only need to characterize the excitation pulse in terms of center frequency ($f_c = 2.5$ GHz) and bandwidth ($BW = 2$ GHz). The pulse uses a Hanning spectral window (*27*), as shown in figure 3. Notice that the total bandwidth of the pulse (between the zero-crossing points) is 4 GHz. However, the value of 2 GHz listed above represents the effective pulse bandwidth (for a definition of the effective pulse bandwidth, see reference [*28*]). We picked such a high value for the pulse bandwidth in order to obtain a very fine radar downrange resolution (in this case, 7.5 cm). To obtain the radar range profiles we start with the frequency domain scattering data, apply the spectral window and take an inverse Fast Fourier Transform (FFT). Then, we compute the envelope of the bipolar time-domain waveform and convert the time scale to spatial downrange. The magnitude is always presented in dB scale.



(a)                                                     (b)
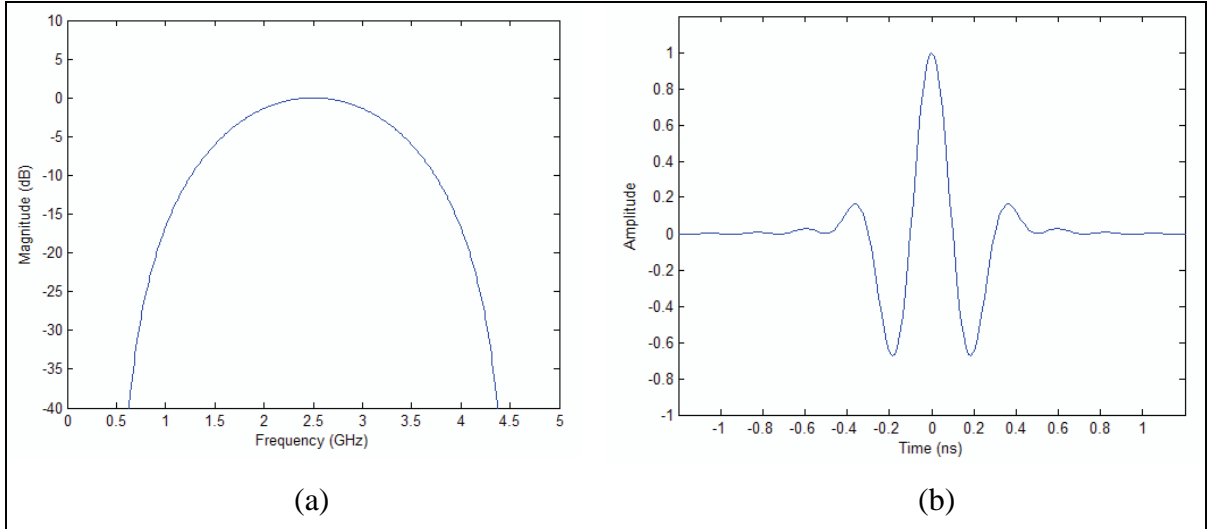
Figure 3. UWB pulse defined by a Hanning frequency window with the center frequency at 2.5 GHz, showing (a) the pulse spectrum and (b) the pulse in the time domain; the total bandwidth extends from 0.5 to 4.5 GHz, while the effective bandwidth is only 2 GHz around the center frequency.

In section 3.5 we analyze a different scenario, where the radar is elevated at an angle of 20°. For this case, we use a slightly different room geometry, described in figure 4. This room has exactly the same dimensions as the one shown in figure 1, however, in this case, we do not include a human inside the room and the floor and ceiling are changed. Thus, the floor becomes an infinite ground plane (since the ground bounce of the incident and scattered plane waves plays a crucial role in the overall radar return; the ground plane is represented in blue), whereas the ceiling is made by a 1" thick slab of sheetrock (we want the ceiling to be easily penetrable so the radar can "see" inside the room; the ceiling appears in yellow). The material dielectrics are: for the ground $\varepsilon_r = 6.8$, $\sigma = 0.1$ S/m (for FDTD) or $\varepsilon' = 6.8$, $\varepsilon'' = 0.9$ (for Xpatch); for the ceiling $\varepsilon_r = 1.8$, $\sigma = 0$ S/m (for FDTD) or $\varepsilon' = 1.8$, $\varepsilon'' = 0$ (for Xpatch). For this scenario, we consider 12" thick brick walls. The excitation pulse parameters are the same as for the previous cases.
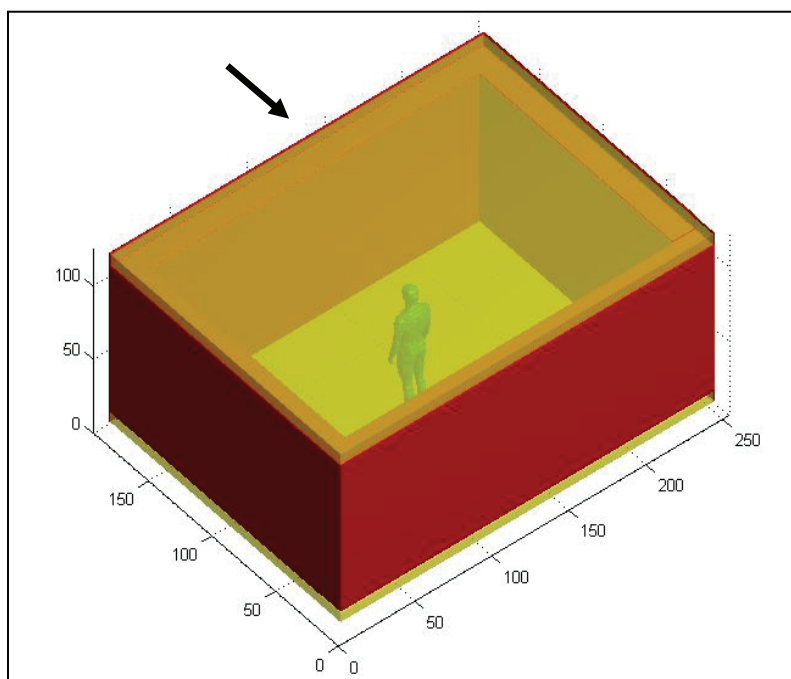
6
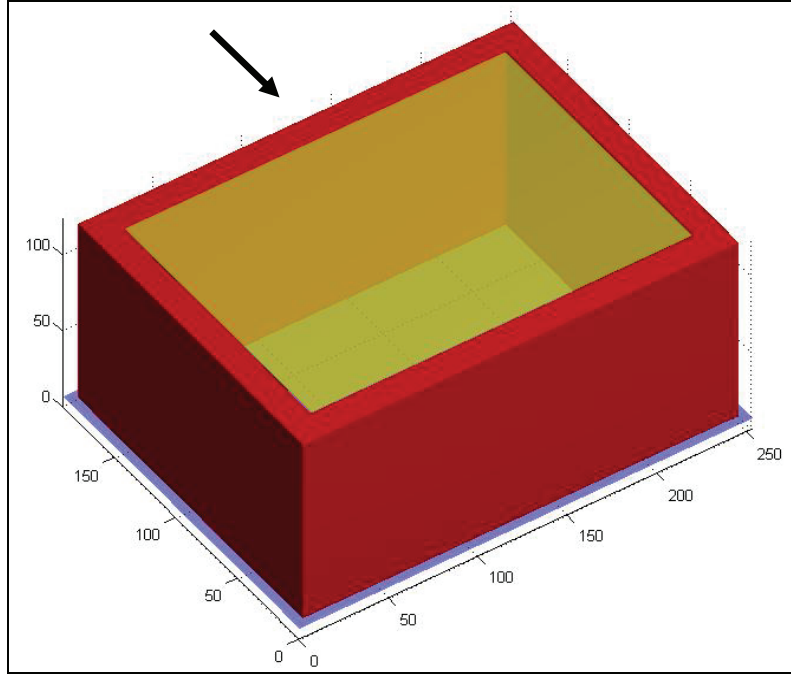
Figure 4. Geometry of the room used in calculating the radar range profiles
in section 3.5; the exterior dimensions are identical with the room
in figure 1, with 12 in. thick walls; the mesh includes an infinite
ground plane and a 1 in. thick ceiling.

### 3.2. Basic FDTD Simulations at Broadside Incidence

In this section, we focus only on FDTD models of the room with a human inside, at 0° elevation. In the range profile plots, we use the following color conventions: dark blue represents the room without ceiling and floor (FDTD models), red represents the room with ceiling and floor (FDTD models), cyan represents the room without the human inside (FDTD models) and black represents the Xpatch results (for that case we always have a human inside and the ceiling and floor do not matter). Also, we overlay the mesh contours (green lines) on top of the range profile, in order to associate the radar signature features to specific scattering centers. For broadside incidence, the mesh contours contain the outline of the front and back walls and the human (as seen from the top), in the middle of the chart.

In figures 5 and 6 we perform a detailed analysis of the brick wall room range profiles, for vertical-vertical (V-V) polarization. In the plots in figure 5, we did not include a floor and a ceiling to the room in order to reveal the artifacts created by this kind of scenario. As we can notice in the figure, most of the peaks in the range profile are easily identifiable with simple or multiple reflections from the walls and the human. We notice that, after transmission through the first wall, all the subsequently reflected pulses are delayed relative to the corresponding target positions, since the waves are slowed down when they propagate through the wall

7

material. A simple calculation can show that the downrange displacement of the pulses that are subject to a round-trip transmission through the front wall is:

$$D = t\left(\sqrt{\varepsilon_r} - 1\right) \tag{1}$$

where $D$ is the displacement (spatial lag), $t$ is the wall thickness and $\varepsilon_r$ is the wall dielectric constant. (Note: in fact, the exact transmission delay equation should include another factor involving the loss tangent, or $\varepsilon''/\varepsilon_r$. However, for all the materials considered in this report, this ratio is relatively low, and equation 1 is accurate within less than 1% error). For peak #2 in figure 5 we obtain $D = 7.6''$ (with respect to the back side of the front wall), which is in complete agreement with the range profile in that figure. Similar evaluations can be made for the other reflected pulses. Peak #3 represents a double round-trip reflection between the two sides of the front wall. Therefore, the distance between peaks #1 and 3 is double the distance between peaks #2 and 3. We also notice a decrease in pulse magnitude upon transmission through walls. The attenuation created by one round-trip transmission is:

$$A(\text{dB}) = 20\log_{10}\left(\frac{1}{T_{12}T_{21}}\exp\left(\pi\frac{tf\varepsilon''}{c\sqrt{\varepsilon_r}}\right)\right) = 40(\log_{10} e)\pi\frac{tf\varepsilon''}{c\sqrt{\varepsilon_r}} + 20\log_{10}\left(\frac{1}{T_{12}T_{21}}\right) =$$
$$1.82\times10^{-7}\frac{tf\varepsilon''}{\sqrt{\varepsilon_r}} + 20\log_{10}\left(\frac{1}{T_{12}T_{21}}\right) \tag{2}$$

where $A$ is the attenuation (in dB), $f$ the frequency, $c$ the speed of light, $\varepsilon''$ the imaginary part of the permittivity, and $T_{12}$ and $T_{21}$ are the air-wall and wall-air transmission coefficients (*29*) (in this formula the wall thickness $t$ must be expressed in meters, and the frequency in Hertz). For the parameters in figure 5, we obtain $A = 12.4$ dB (at the pulse center frequency), which matches the difference in magnitude between peaks #1 and 2 or between peaks #5 and 6 (the transmission coefficient term contribution is about 1 dB in this case). The human contribution to the range profile is easy to identify as the difference between the graphs obtained in the presence of the human and in its absence (peak #10). However, there are a number of pulses in the range profile (peaks #7 through 9) that require more complex explanation.
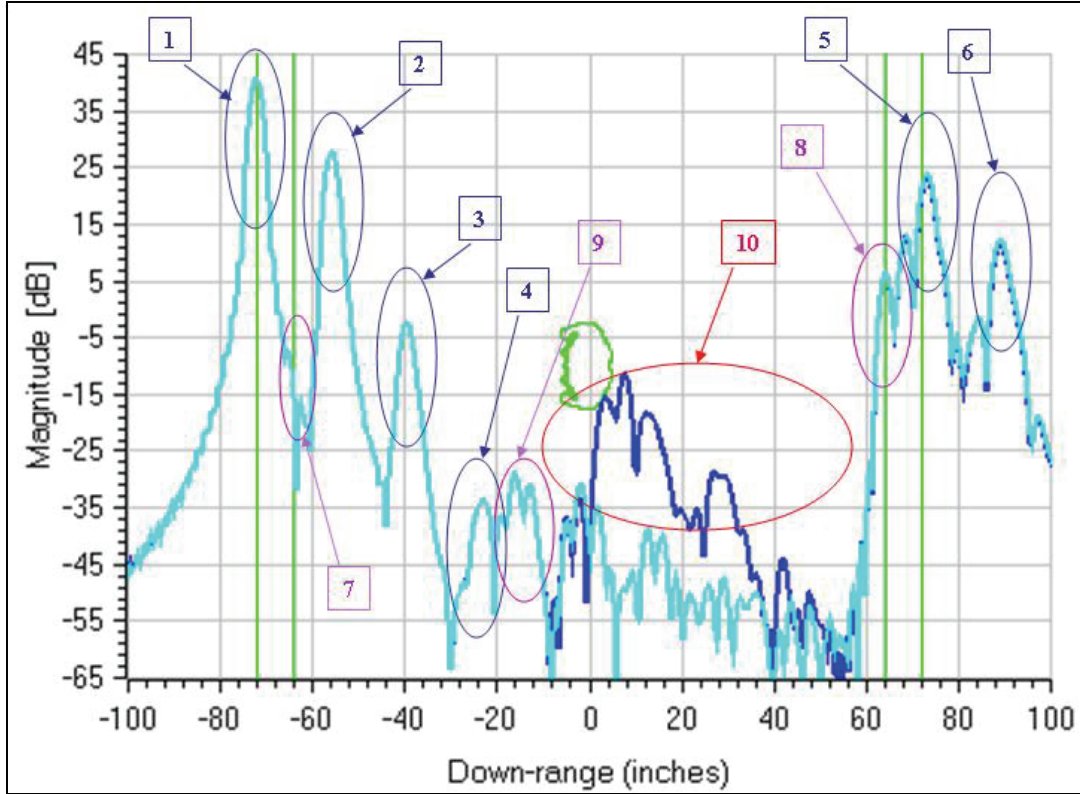
NOTES:
    (a) In all range profiles, the contours of the room and human meshes are overlaid in green.
    (b) The numbered peaks have the following origins:
        1 – reflection from the front side of the front wall
        2 – reflection from the back side of the front wall
        3 – double round-trip reflection from the back side of the front wall
        4 – triple round-trip reflection from the back side of the front wall
        5 – reflection from the front side of the back wall
        6 – reflection from the back side of the back wall
        7 – diffraction off the trailing edge of the front wall
        8 – diffraction off the leading edge of the back wall
        9 – multiple diffraction off the front wall
        10 – human contribution

Figure 5. FDTD-computed radar range profiles for a brick room similar to that described in figure 1, where the ceiling and floor have been removed; in light blue, the room alone (no human inside); in dark blue, the room with the human inside; V-V polarization, broadside incidence.

9

It can be shown that peaks #7 and 8 are produced by diffraction over the top and the bottom of the front and back walls. The main diffraction mechanisms are illustrated in figure 6. We notice that the top and bottom of each wall forms a 90° edge that scatters energy in all directions. Some of the diffracted energy propagates over these edges back to the receiver. It is interesting that, although the peak #7 (coming from the trailing edge of the front wall) is almost negligible as compared to peaks #1 and 2, peak #8 (coming from the leading edge of the back wall) is comparable in magnitude with peaks #5 and 6. This effect can be explained by the fact that a leading 90° edge produces a relatively strong backscatter return at grazing incidence (compared to a trailing edge (*29*), which produces peak #7), and also because the propagation of peak #8 back to the receiver goes entirely through air, over the top or bottom of the room (as opposed to peaks #5 and 6, which must penetrate at least one wall on their way back to the receiver). This diffraction over the top/bottom of the walls mechanism is made possible by the fact that we use plane waves at grazing incidence (0° elevation) in our FDTD models. In a real ground-based radar system, the antenna would have a relatively wide fanning pattern, and therefore, the incident waves would not propagate at grazing incidence over the top of the walls. Consequently, this kind of diffraction mechanism is not possible in a real radar system, even in the case when we have a building without ceiling.
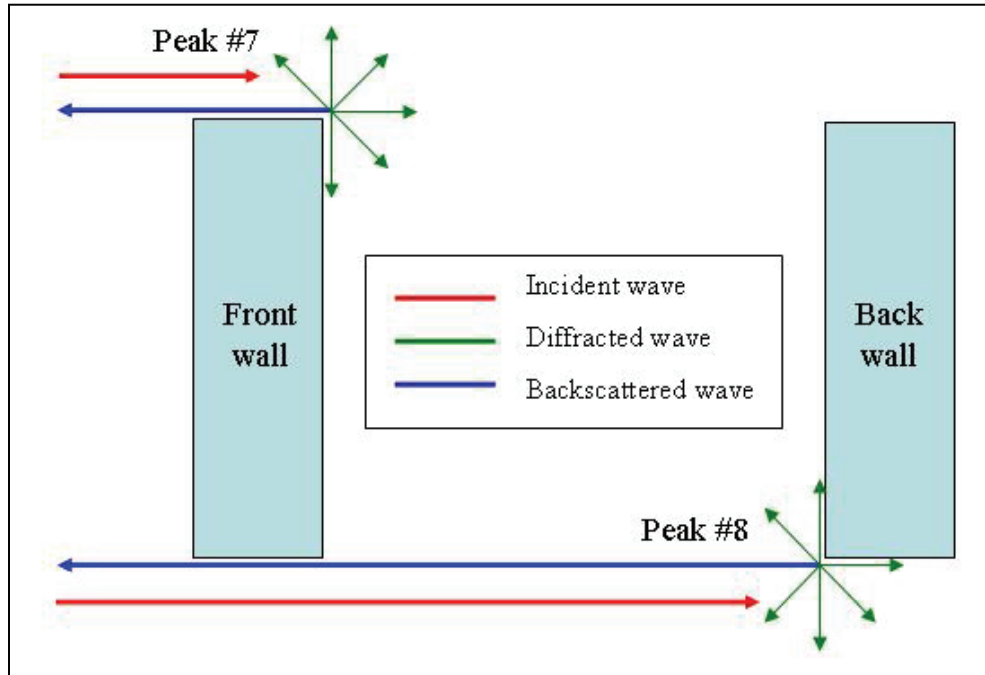


Figure 6. Schematic representation of the diffraction mechanisms accounting for peaks #7 and 8.

We conclude that these diffraction-produced peaks in the range profiles are FDTD modeling artifacts that do not reflect the operation of a real-life radar system. In order to eliminate them, we must add a floor and a ceiling to the room, as shown in figure 1 (the thickness and building material for these two are not critical parameters). The new range profiles obtained in figure 7 demonstrate the elimination of peaks #7 and 8 through this technique. Moreover, peak #9, which we ignored in the previous paragraph, also disappears in figure 7. Although we do not have a precise explanation for the origin of this peak, the plots in figure 7 suggest that it is also related to diffraction (multiple diffraction most likely) from the front wall's edges. We should also mention that this diffraction over the top/bottom of the walls is not a problem for the Xpatch models (even if we omit the floor and the ceiling), since Xpatch cannot account for diffraction over dielectric edges aligned as in figure 6.



Figure 7. FDTD-computed radar range profiles for the brick room in figure 1, with the human inside, in V-V polarization, broadside incidence; in dark blue blue, the room without ceiling and floor; in red, the complete room as in figure 1.

11

Figure 8 compares the range profiles of a room with and without covers (ceiling and floor), when the walls are made of concrete. In t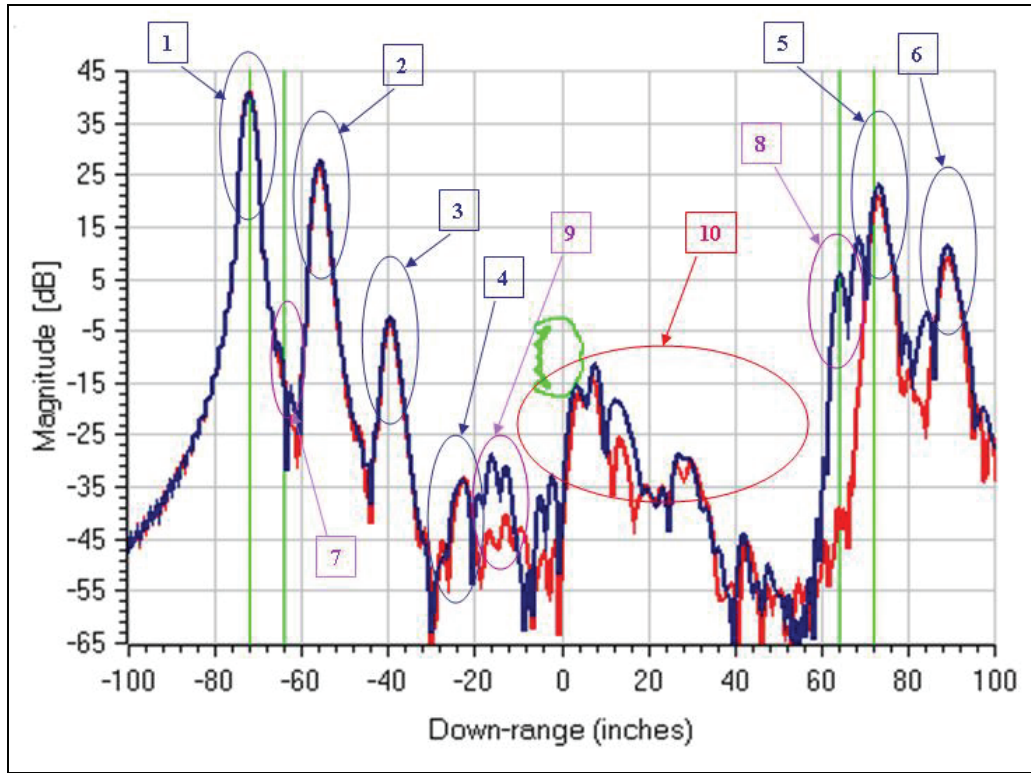hese plots, we notice that the downrange lags of the pulses subject to wall transmission are larger than in the case of the brick walls, because of the higher dielectric constant of concrete (the displacement for one round-trip transmission is 12.9" according to equation 1). Also, the attenuation upon wall transmission is larger because of the higher loss (conductivity) exhibited by concrete (34 dB for one round-trip transmission, according to equation 2). Again, we notice the diffraction over the top/bottom of the walls for the room without floor and ceiling. The second diffraction peak (#8) is particularly large (in fact larger than the corresponding peak for the brick walls), since, as explained before, the propagation of the diffracted waves goes entirely though air, and not through the walls. Moreover, there is another diffraction peak (#11) that corresponds to the trailing edge of the back wall, which displays a sizeable magnitude. As in the case of the brick walls, introducing the floor and the ceiling eliminates the diffraction problem, including the peak #9 which is likely produced by multiple diffraction over the front wall.
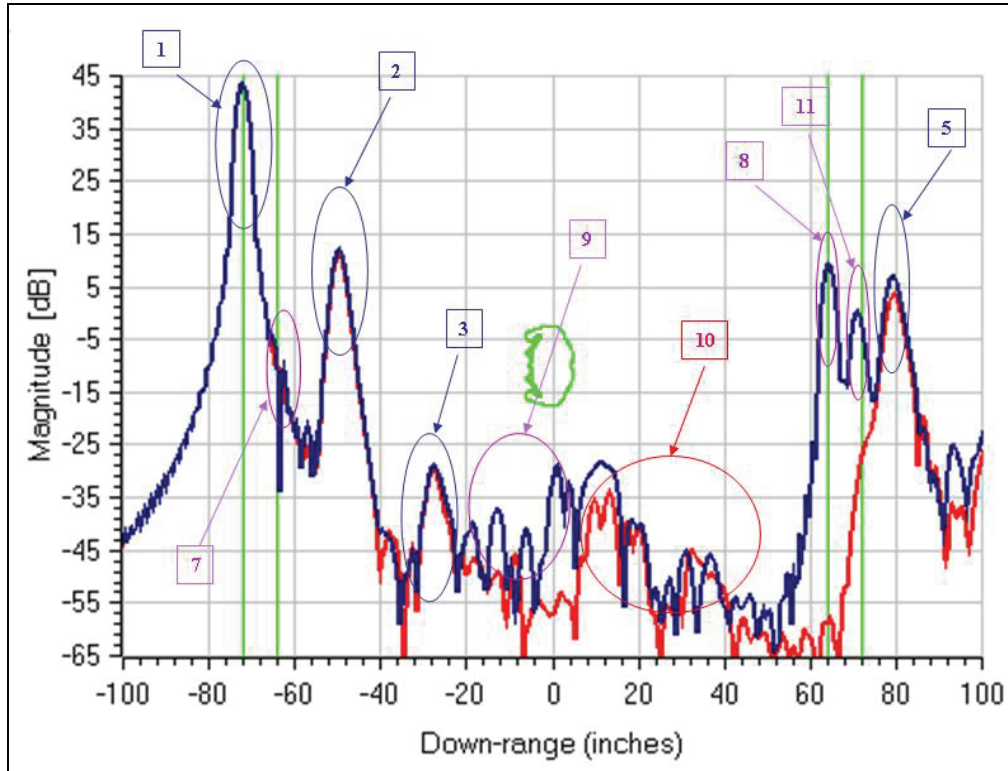


Figure 8. FDTD-computed radar range profiles for the concrete room in figure 1, with the human inside, in V-V polarization, broadside incidence; in dark blue blue, the room without ceiling and floor; in red, the complete room as in figure 1.

In figures 9 through 11, we plot the room range profiles as computed by FDTD at broadside incidence, after cleaning up all the modeling artifacts. In each case, we compare the range profiles of the room with and without human inside, in order to emphasize the human contribution as the difference between the two graphs. We perform this analysis for both co-polarization combinations (V-V and horizontal-horizontal (H-H)).

12

Figure 9. FDTD-computed radar range profiles for the brick room in figure 1, at broadside incidence, showing: in light blue the room without the human; in red the room with the human, for (a) V-V polarization and (b) H-H polarization.



Figure 10. FDTD-computed radar range profiles for the concrete room in figure 1, at broadside incidence, showing: in light blue the room without the human; in red the room with the human, for (a) V-V polarization and (b) H-H polarization.
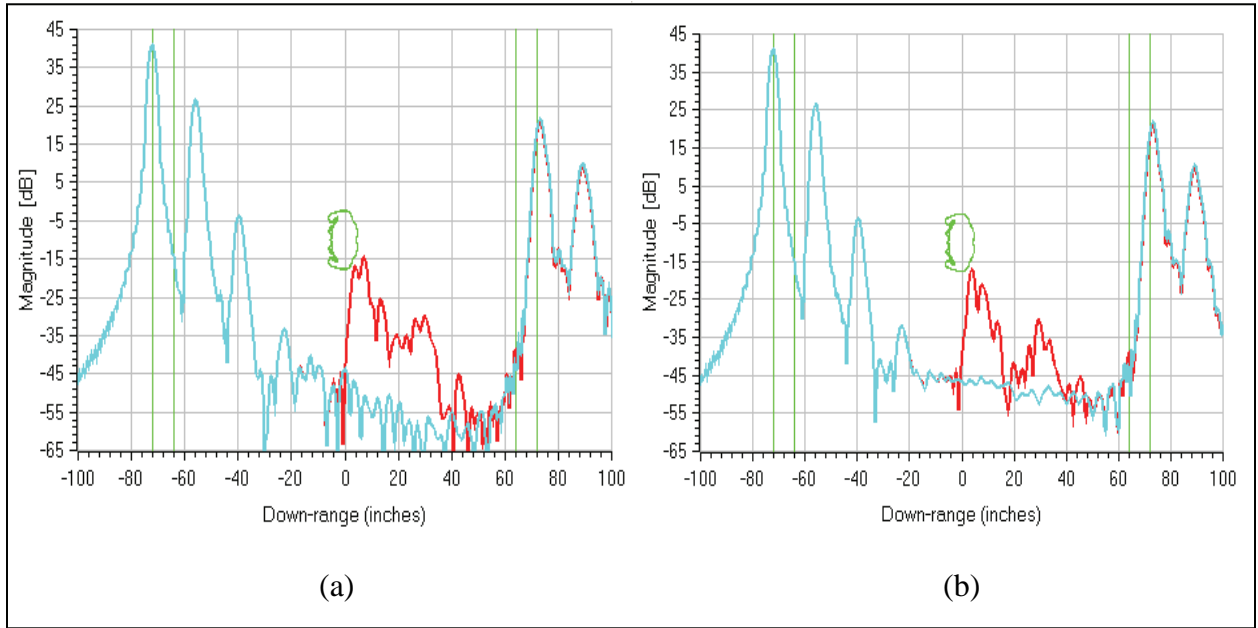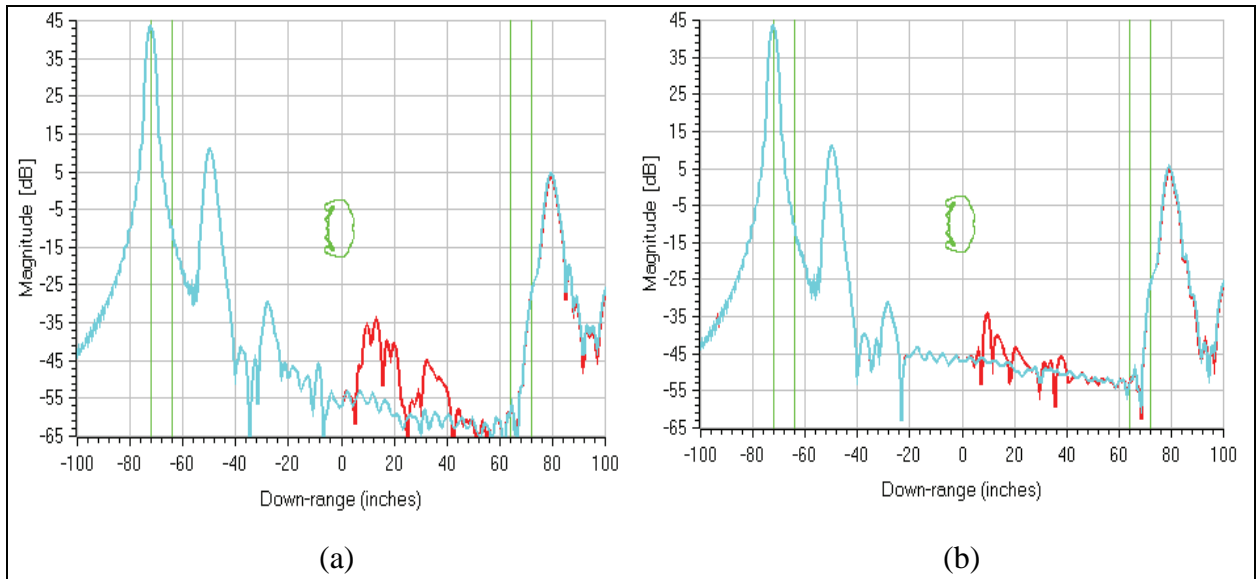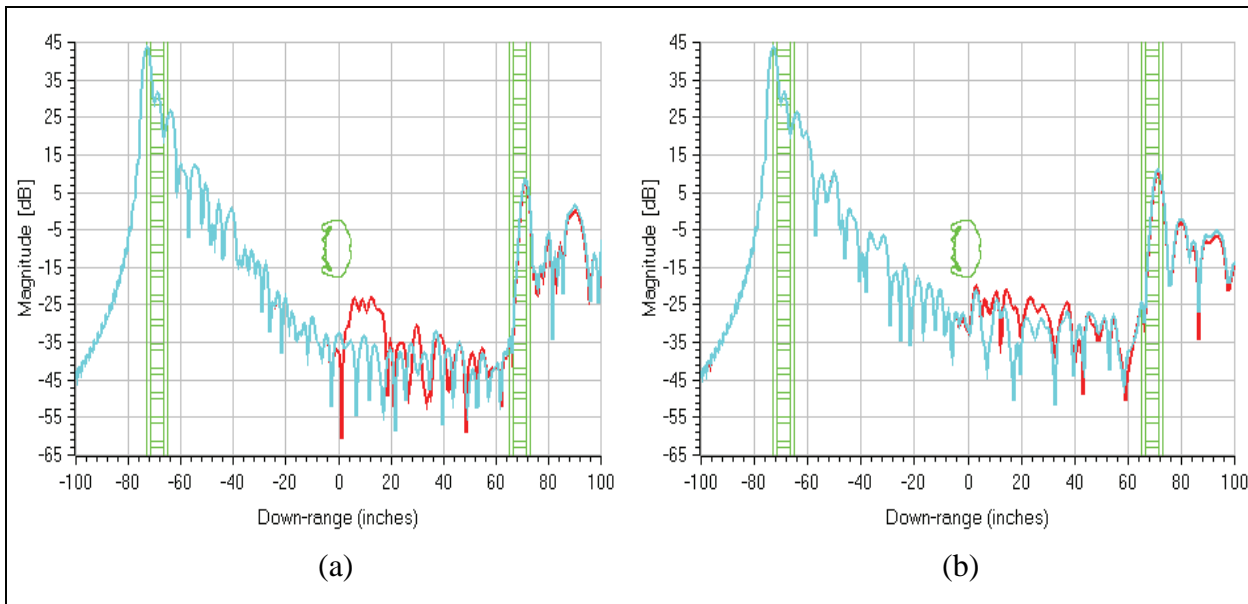
Figure 11. FDTD-computed radar range profiles for the cinder block room in figure 1, at broadside incidence, showing: in light blue the room without the human; in red the room with the human, for (a) V-V polarization and (b) H-H polarization.

The range profiles for the brick and concrete rooms (figures 9 and 10) were already described in the previous paragraphs. Besides, there are no significant differences between the V-V and H-H polarizations, except for the fact that the numerical noise floor seems to be higher for the H-H case. This could present a problem when we have to deal with a very weak return from targets placed behind walls (such as in figure 10b), because the high level of noise would prevent detection of such targets. However, it should be emphasized that this is strictly a modeling issue, and it has absolutely no correlation with the noise figures of a real radar system (figure 10b indicates a dynamic range for our FDTD implementation of about 90 dB, which, according to the literature, is a very good figure for this type of algorithms [17]). Also, we notice that the human body response is very similar for the two polarizations (consistent with the results in [4]).

The cinder block case, shown in figure 11, is different from the previous two in the sense that the walls are non-uniform, and we cannot clearly separate the reflections from the planar wall sides any longer. The new electromagnetic phenomena in this case are the multiple reflections that take place inside the air gaps of the cinder blocks. Since many reflections can take place inside the wall before the wave amplitude dies out, we notice these reverberations in the range profiles as a slowly decaying "tail" that appears behind the front wall. This wall-induced clutter can hamper the attempts to detect a target placed in the room. In the scenario depicted in figure 11, the human body return is still above the clutter level. However, for a target placed very close to the front wall, the return would be completely swamped in clutter, making the detection process impossible.

14

## 3.3 FDTD versus Xpatch at Broadside Incidence

Figures 12 through 14 compare the range profiles obtained by FDTD and Xpatch for the same three types of walls. Again, we look at both V-V and H-H polarizations. The human is always included in the mesh.

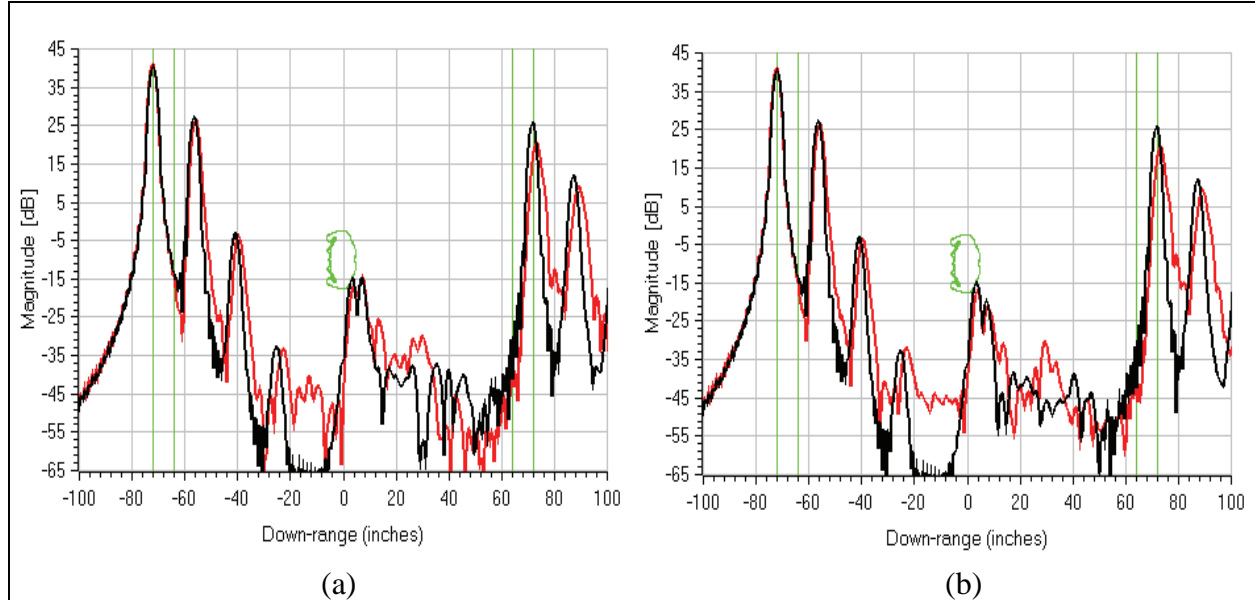

Figure 12. Radar range profiles for the brick room in figure 1, at broadside incidence, as computed by FDTD (red line) and Xpatch (black line), for (a) V-V polarization and (b) H-H polarization.
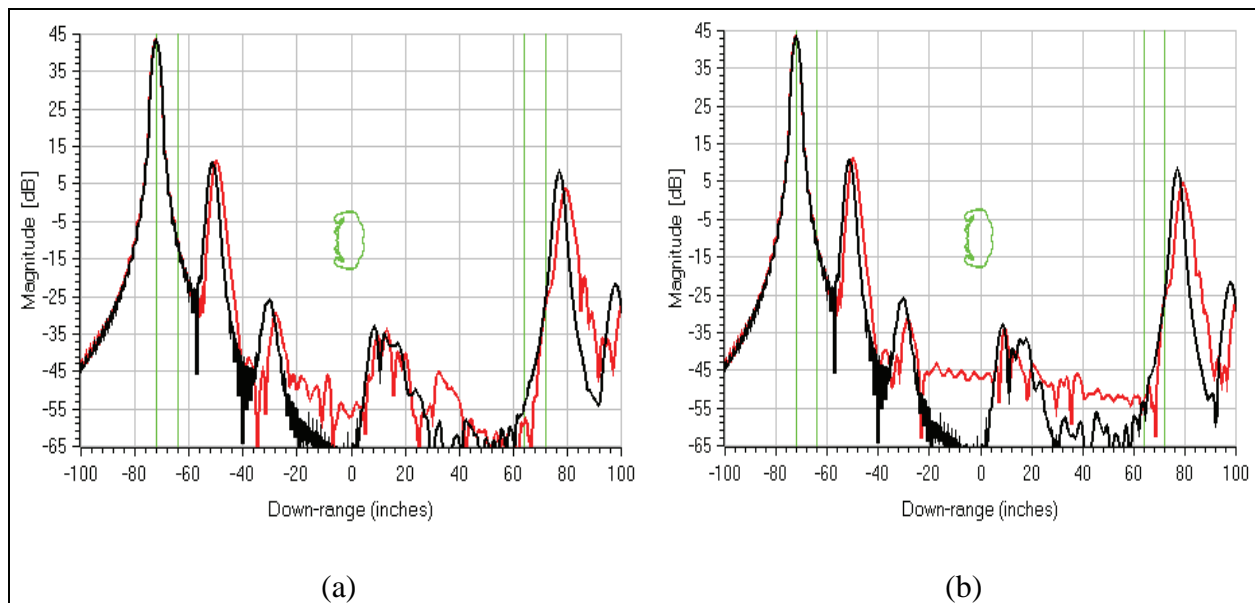


Figure 13. Radar range profiles for the concrete room in figure 1, at broadside incidence, as computed by FDTD (red line) and Xpatch (black line), for (a) V-V polarization and (b) H-H polarization.
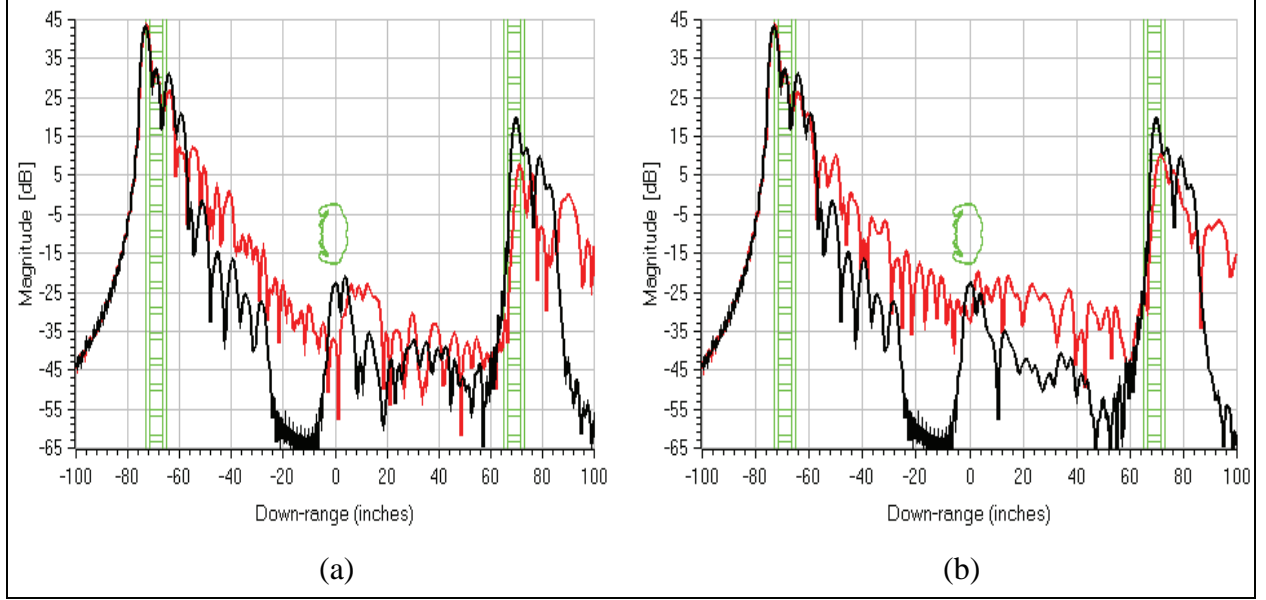
Figure 14. Radar range profiles for the cinder block room in figure 1, at broadside incidence, as computed by FDTD (red line) and Xpatch (black line), for (a) V-V polarization and (b) H-H polarization.

Figures 12 and 13 (brick and concrete walls) show a good agreement between the two modeling codes. The most important differences that we notice are small phase lags between some of the peaks computed by the two methods. These lags become more pronounced for the late-time peaks, and they are more significant for the concrete walls than for the brick walls. The difference can be explained by the numerical dispersion present in the FDTD algorithm (*17*) (Xpatch does not exhibit this problem, so it correctly evaluates the phase of each peak). This phenomenon is dependent on the spatial sampling rate of the EM fields. For instance, inside the brick walls, the sampling rate at 3.5 GHz (the upper limit of the excitation pulse's 6 dB frequency band) is about 9 samples per wavelength, whereas inside the concrete walls, this drops to about 6.6 samples per wavelength. In consequence, our simulations do not strictly meet the well-known rule of thumb of at least 10 samples per wavelength at the highest frequency in the spectrum, in the densest medium (*17*). While this may not be a critical issue when the propagation distance through the high-dielectric medium is short (in our case, the front and back walls), the results in figures 12 and 13 demonstrate that some phase errors occur in the FDTD models. At the same time, we would like to emphasize that our FDTD grid resolution of 5 mm was limited by considerations related to the computational domain size – a smaller cell size would have led to a significantly increase in the computational resources necessary to model this scenario.

Also, some differences in the range profiles come from FDTD's much higher numerical noise floor. However, as mentioned before, this is not an essential issue, since the numerical noise has no relationship with a real radar system noise.

16

Nevertheless, in the cinder block case (figure 14) we notice more significant deviations between the two modeling methods. Specifically, Xpatch underestimates the clutter produced by multiple reverberations of the radar waves inside the front wall. This suggests the fact that there are more subtle phenomena occurring inside the cinder blocks, such as multiple diffraction (which cannot be taken into account by Xpatch), with significant contribution to the radar return.

In this section, we also compare the human contribution to the range profiles obtained by the two methods. In figure 15 we plot the radar return of a human placed in free-space and facing the radar (this is the reference for how close the two methods perform in modeling the human in a clutter-free environment). We notice that the FDTD and Xpatch range profiles match fairly well, especially in the main response (produced by the front of the human). Some differences can be seen in the late-time response, where Xpatch does not account for some multiple reflection phenomena (for more details on this issue see reference [4]). The graphs in figure 16 are zoomed-in portions of the range profiles in figures 12a and 13a, respectively (V-V polarization only). They compare the human contribution computed with the two modeling methods, for the brick and concrete rooms, respectively. Again, the match is fairly good, especially in the main response, with the same kind of differences in the late-time response as mentioned above. Some differences between the plots in figure 16a and b are produced by the higher numerical noise floor of the FDTD algorithm as compared to Xpatch.
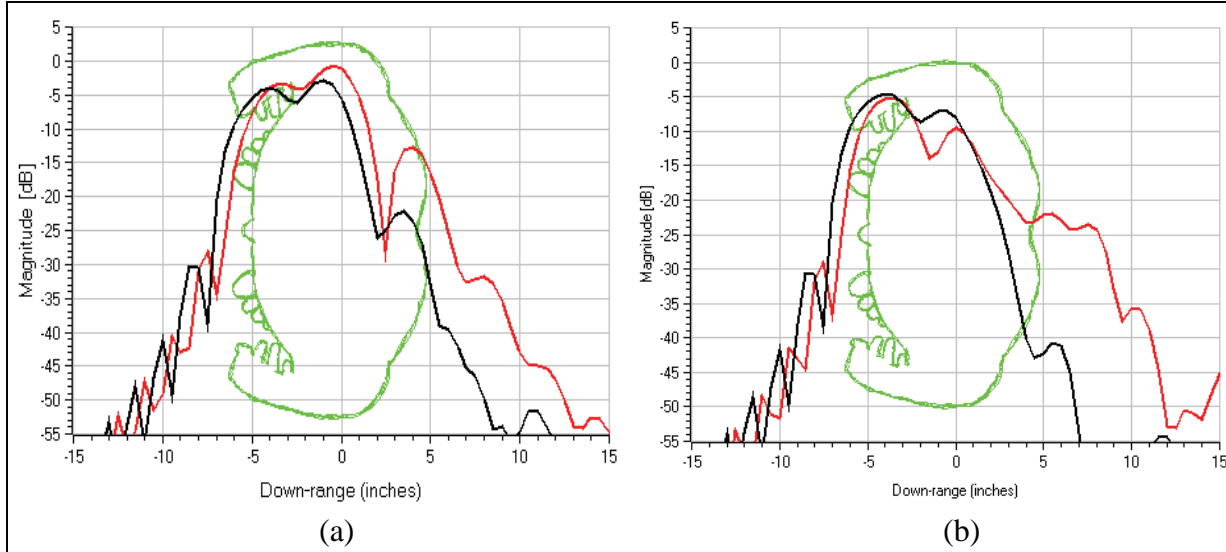


Figure 15. Radar range profiles of the fit man in free-space, as computed by FDTD (red line) and Xpatch (black line), for (a) V-V polarization and (b) H-H polarization.
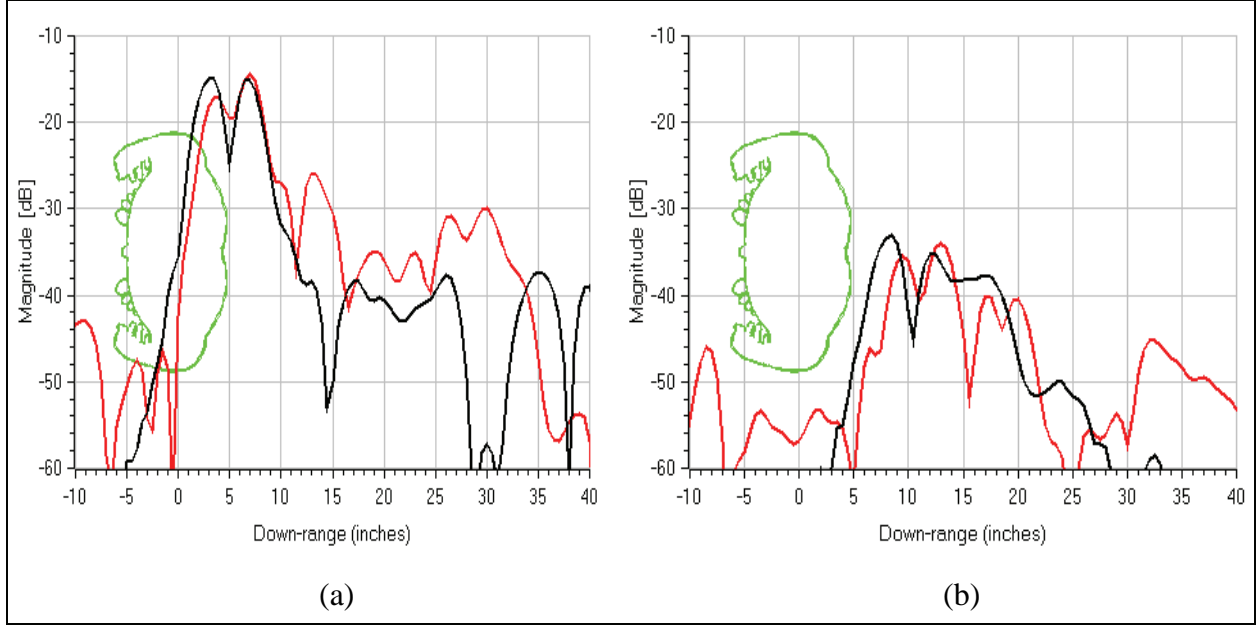
Figure 16.  Detail on the radar range profiles for the room in figure 1, as computed by FDTD (red line) and Xpatch (black line), in V-V polarization, at broadside incidence, for (a) brick walls and (b) concrete walls.

### 3.4.  FDTD versus Xpatch at Oblique Incidence

In this section, we continue the comparison between the FDTD and Xpatch range profiles of a room with a human inside, by looking at oblique incidence in the azimuth direction (the elevation angle is still 0°).  In order to avoid complications, we only analyze the brick room for this type of incidence.  In figures 17 and 18, we represent the range profiles for 0° (as reference), 15°, 30°, and 45° incidence in azimuth, for V-V and H-H polarizations, respectively.  Although the match in the main peaks between the two solutions is excellent at 0°, we notice that the two methods start to diverge at oblique incidence, the larger the off-broadside angle, the higher the deviation (again, there are differences in the numerical noise floor, but we are mainly interested in the peaks).  It is interesting to notice that the deviation is larger for the H-H polarization than for V-V.
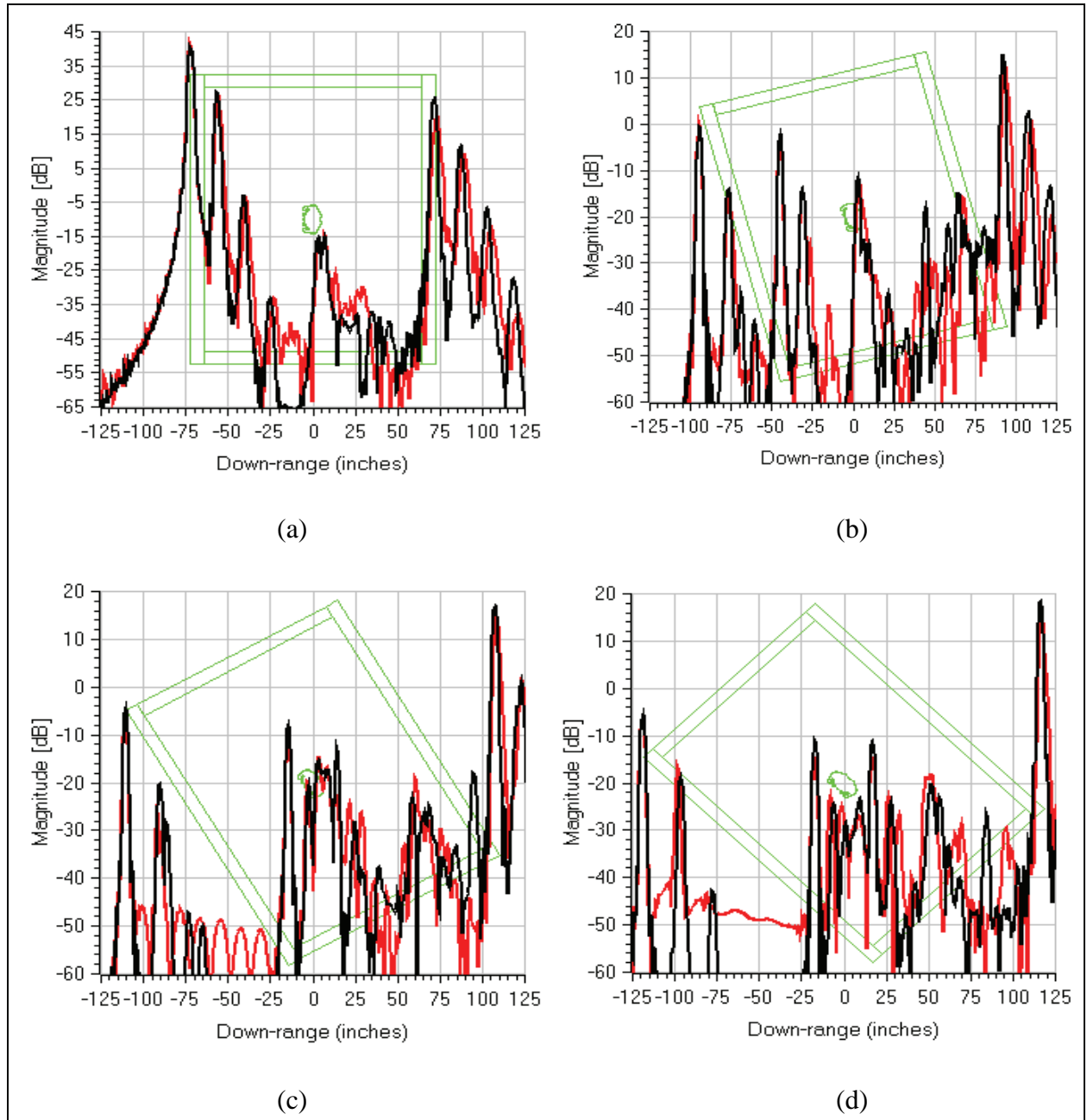
18

Figure 17. Radar range profiles for the brick room in figure 1, as computed by FDTD (red line) and Xpatch (black line), in V-V polarization, for (a) 0° azimuth (b) 15° azimuth (c) 30° azimuth, and (d) 45° azimuth.
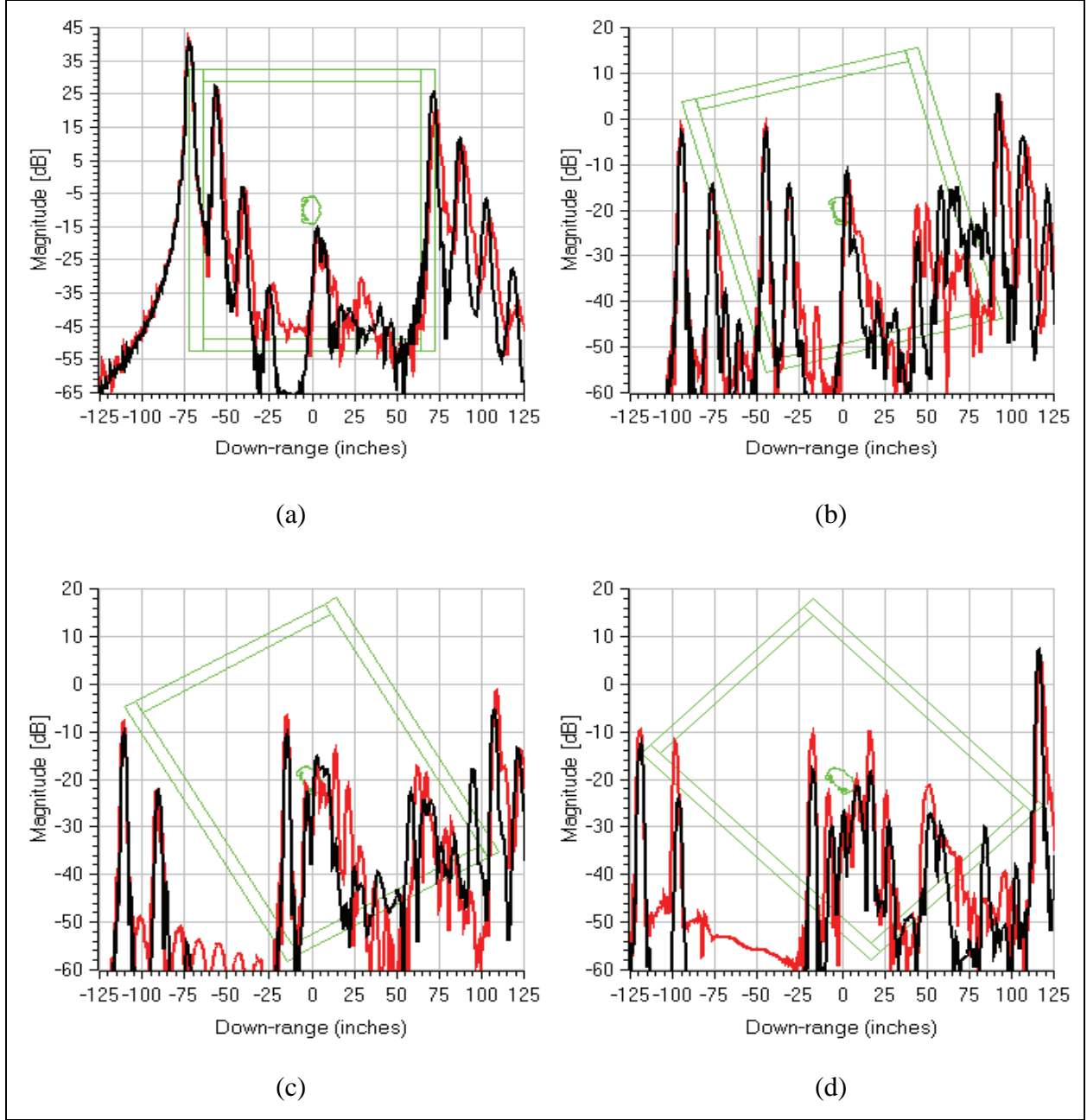
Figure 18. Radar range profiles for the brick room in figure 1, as computed by FDTD (red line) and Xpatch (black line), in H-H polarization, for (a) 0° azimuth (b) 15° azimuth (c) 30° azimuth, and (d) 45° azimuth.

In order to explain the difference between the FDTD and Xpatch solutions at oblique incidence, we must first notice that most of the major peaks in the range profiles come from diffractions from the room's corners (both interior and exterior corners). The problem of electromagnetic wave diffraction from a dielectric wedge does not have a general analytic solution (*30*); therefore, a treatment of this phenomenon could not be incorporated as such in Xpatch. Consequently, for scattering off the room's corners, the Xpatch solution must rely on a superposition of PO integrals computed on the walls sides, which are known to produce errors in non-specular directions of observation (*20*). It is interesting to notice, however, that Xpatch can

accurately treat diffraction from edges made of perfect electric conductor (PEC), since a closed-form analytic solution for this case does exist (*30*).  Xpatch incorporates a switch that allows the user to turn the PEC edge diffraction terms computation "on" or "off" (turning the diffraction switch "on" may significantly increase the run time, so there are cases where the increase in solution accuracy does not justify the added computational expense).

We demonstrate the difference between the Xpatch calculations with and without diffraction terms for a PEC room with the same dimensions, at oblique incidence, in figure 19 (V-V polarization only).  In this case, the walls are impenetrable, so the main radar return comes from the exterior corners (main peaks in figure 19).  The FDTD (reference) solution displays a more complicated structure:  besides the main peaks we see additional late-time responses, which are produced by surface waves traveling along the PEC wall faces (*20*).  Again, this phenomenon is not captured by Xpatch. However, its effect is irrelevant for real walls made of lossy dielectric. In comparing the main peaks, we notice that the two solutions are off by up to 7 dB in figure 19a (diffraction switch turned "off"), but they match very well in figure 19b (diffraction switch turned "on").  It should be mentioned that the analytic solution computed by GTD (*29*) produces exactly the same main peaks as in figure 19b.
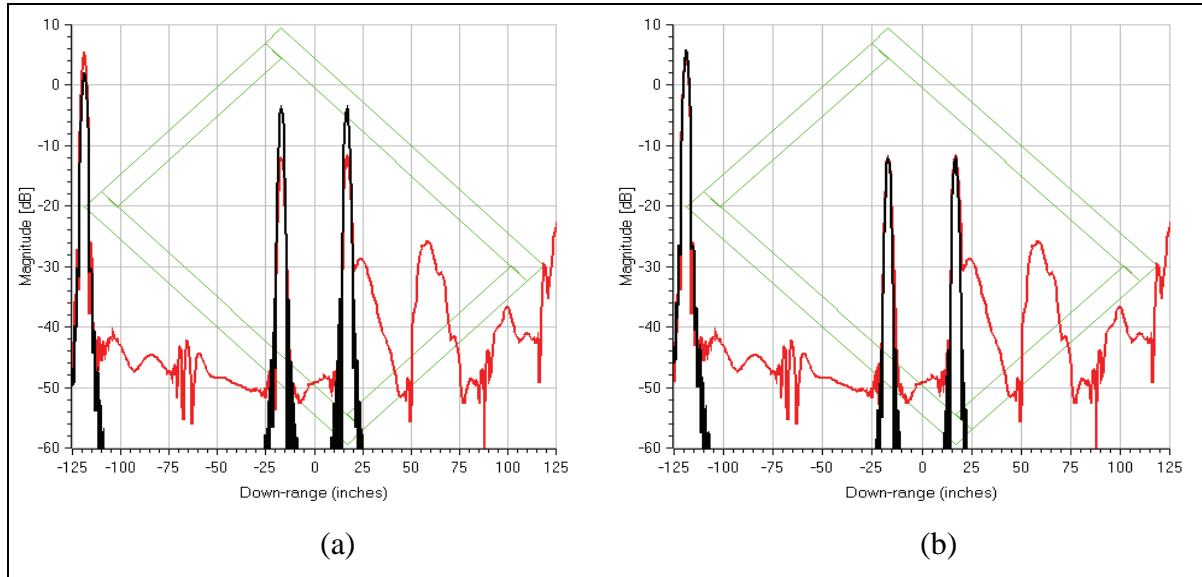


Figure 19.  Radar range profiles for a room as in figure 1, with metallic walls, as computed by FDTD (red line) and Xpatch (black line), in V-V polarization, for 45° incidence.

Although this analysis of a room with PEC walls is not directly relevant to our STTW radar problem, it helps us understand where the Xpatch problems for the room models at oblique incidence (figures 17 and 18) come from.  The conclusion is that the errors originate in the inadequate treatment of diffraction produced by the dielectric wall edges.

### 3.5.  FDTD versus Xpatch for an Airborne Radar Scenario

So far, all models have assumed a ground-based radar, with incidence at $0^0$ elevation.  In this section, we consider incidence at an elevation of $20^0$, which would be more characteristic to an airborne radar scenario.  The room mesh used in this case was described in section 3.1 (and figure 4) – its different features include a penetrable ceiling and an infinite ground plane (floor).  Also, we do not place the human in the room in this case.  The main purpose of this analysis is to assess the accuracy of the Xpatch solution compared to the reference (FDTD) for such a scenario.

In figure 20 we consider incidence at $0^0$ azimuth.  One major contribution for this case is the ground bounce, since the ground plane and the walls make perfect $90^0$ corners.  The third peak in figure 20 (both a and b) is produced by this phenomenon.  It appears more prominently in H-H polarization than in V-V polarization (by about 25 dB), because the reflection coefficient is much larger in the former case (this can be related to the existence of the Brewster angle for V-V polarization (29), close to the actual elevation incidence angle that we picked for this scenario).  By comparing the Xpatch and FDTD solution, we notice a good match in the main peaks, although the solutions start to diverge in the late-time.  As explained in section 3.5, Xpatch produces errors for off-broadside incidence to the walls, where diffraction terms become significant.  Moreover, in the case considered here, these diffraction terms interact with the ground plane, creating a complex structure of the radar return.



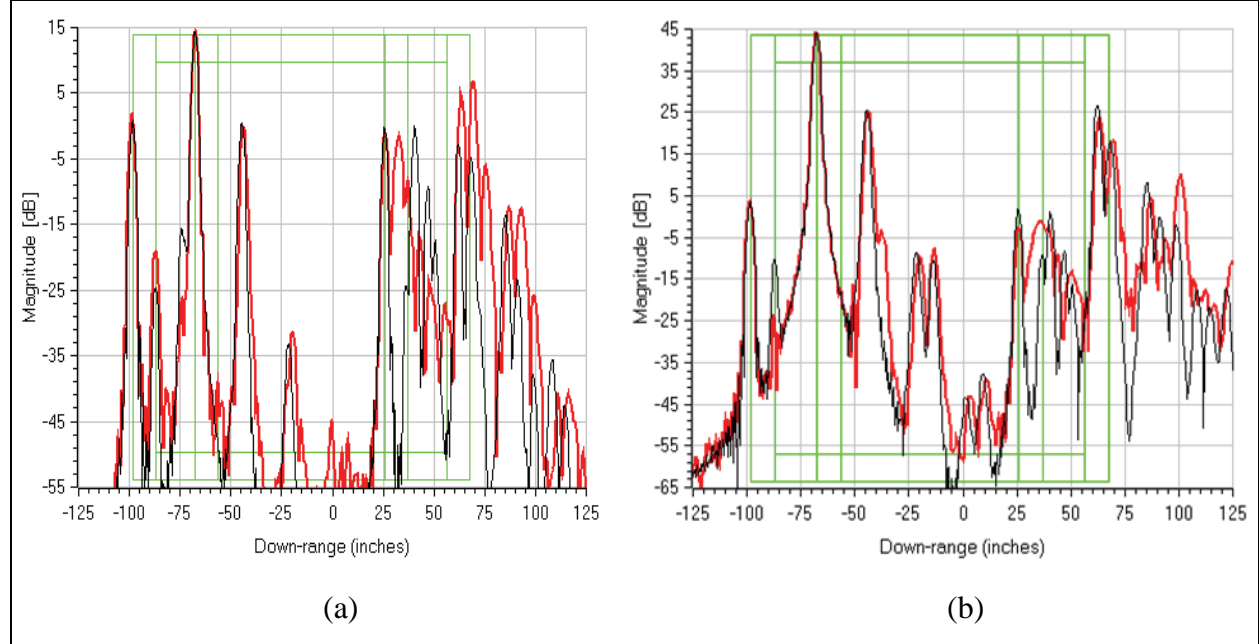(a)                                                                (b)

Figure 20.  Radar range profiles for the brick room in figure 4, as computed by FDTD (red line) and Xpatch (black line), at 0° azimuth and 20° elevation, for (a) V-V polarization and (b) H-H polarization.

Finally, in figure 21 we tilt both directions of incidence by making $\phi = 30°$.  This time the mismatch in the main peaks becomes more significant, with differences up to 10 dB for H-H

polarization. The principal scattering centers in this case are vertices and trihedrals made by dielectric surfaces (usually combined with the ground bounce), for which we expect Xpatch to exhibit even worse accuracy than in the previous cases.
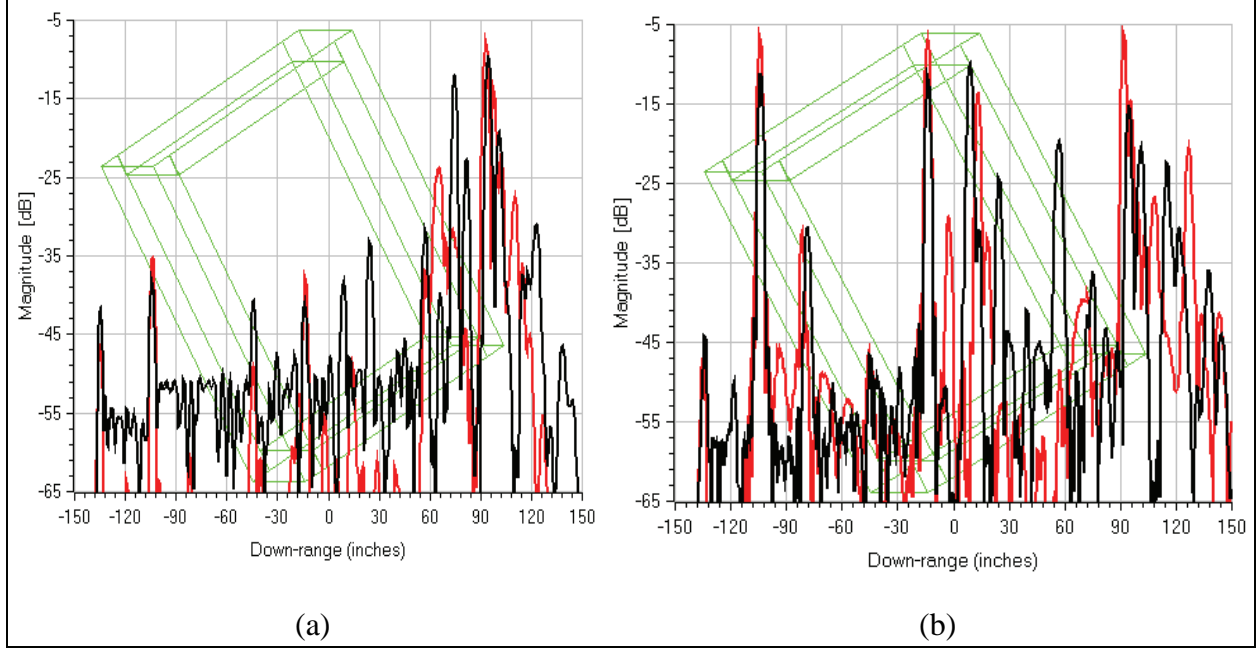


Figure 21. Radar range profiles for the brick room in figure 4, as computed by FDTD (red line) and Xpatch (black line), at 30° azimuth and 20° elevation, for (a) V-V polarization and (b) H-H polarization.

## 3.6. Modeling the Radar in Cross-Polarization

In this section we introduce the idea that operating a STTW radar system in cross-polarization mode could enhance the contrast between the human and the walls or surrounding objects. The phenomenological basis for this idea is that both reflection from a flat surface and diffraction from straight edges produce a null response in the backscatter direction in cross-polarization (*29*). However, since the human body presents a curved, irregular shape, it should create a larger cross-polarized radar return than walls or other objects with regular, straight-edged, right-angled shapes. This would provide the opportunity to reduce the wall signature in the radar received waveform while emphasizing the human's response, and at the same time could provide a way to discriminate the signature of a human from that of other objects with the particular shapes mentioned above.

We consider again the same room as in figure 1, with an incidence elevation angle of $0^0$. Since the mesh is symmetric over the *x-z* plane, incidence at $0^0$ azimuth would produce null cross-polarization fields in backscatter (*20*). Therefore, we choose an oblique azimuth angle of incidence ($\phi = 30^0$). In figure 22 we compare, side by side, the range profiles obtained for co-polarization mode (V-V) and cross-polarization mode (vertical-horizontal (V-H)). These simulations were performed with FDTD, since Xpatch does not produce accurate results in cross-

23

polarization (*19*). Whereas the human response is about 15-25 dB below the major peaks produced by the walls in co-polarization (figure 22a), the situation is reversed in the cross-polarization case (figure 22b). Notice though that the magnitude scale in figure 22b is much lower than the scale in figure 22a. Thus, the human response in cross-polarization is still about 20 dB lower than in co-polarization (notice that the attenuation upon transmission through walls is the same in both cases). Consequently, a radar operating in cross-polarization would have to process extremely weak signals, which may be obscured by noise. The authors recognize that there may be other issues related to building and operating a radar system in cross-polarization that are beyond the scope of this report. However, we think this is an idea that deserves further investigation, at least through computer simulations in a first instance.



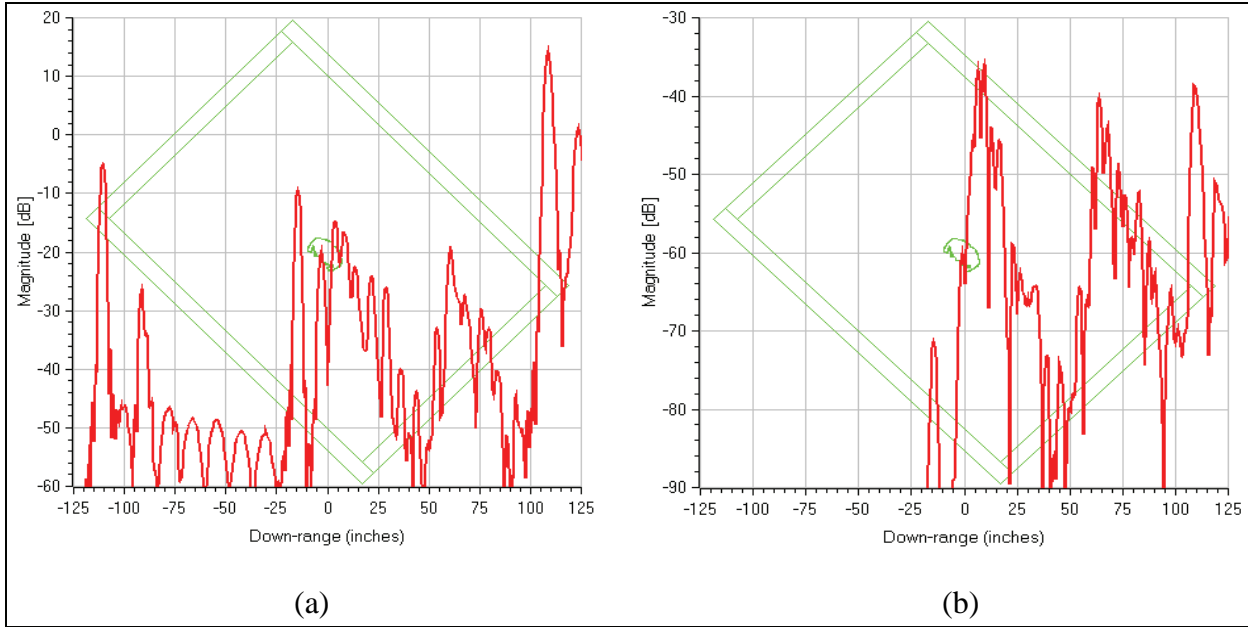(a)                                                                 (b)

Figure 22. FDTD-computed radar range profiles for the brick room in figure 1, for 30° azimuth and 0° elevation, showing (a) V-V polarization and (b) V-H polarization.

## 4.  Conclusions

This study consisted of modeling the radar return from a simple room including a human. For this purpose, we employed two different simulation methods, FDTD (an exact solver) and Xpatch (an approximate solver). The results, presented as radar range profiles with a very large bandwidth, at various angles of incidence, help us better understand the electromagnetic phenomenology in operating an UWB radar for STTW applications. At the same time, we were interested in validating Xpatch as an accurate tool for modeling general STTW radar problems.

We considered three types of wall materials or construction techniques: brick, cinder block and solid concrete. The emphasis was on incidence at 0° elevation, as one would expect from a ground-based radar. One important conclusion was that, in the FDTD simulations, we need to add a floor and a ceiling to the room, in order to avoid certain modeling artifacts (diffraction of the plane waves over the top and bottom of the walls) and make the model more realistic. We also investigated incidence at 20° elevation, characteristic to an airborne radar scenario, where we added an infinite ground floor and an easily penetrable roof made of a thin sheetrock slab. Although in most cases we considered that the radar operates in co-polarization mode, we briefly explored the cross-polarization radar return from the room at oblique incidence, demonstrating that in this case, the human produces a much stronger response relative to the walls (however, in absolute terms, the cross-polarized received signal is much weaker than the co-polarized one).

In terms of chances to detect the human placed in the room, we noticed a relatively large backscatter return from the human when the walls are made of bricks, which do not attenuate the radar waves very severely. In the case of the concrete walls, the attenuation is much more pronounced, and the return from the human is weaker. The cinder block wall case falls in between: although the building material is concrete, the air gaps allow more penetration than a solid concrete wall. However, the interesting effect in this case is produced by multiple reverberations of the radar waves inside the blocks, resulting in a significant amount of clutter within a sizeable range that extends behind the wall. We concluded that, in this case, it would be extremely difficult to detect any kind of target placed in the vicinity of the wall.

By comparing the two modeling methods, we generally obtained a good match in the range profiles, both in terms of amplitude and phase. These results confirm the fact that Xpatch can be confidently used in simulating STTW radar problems, at frequencies as low as 1 GHz. As we have mentioned in a previous study (16), this is made possible because the scattering structure physical dimensions for these scenarios (large walls) are much larger than the wavelength, therefore, the PO approximation works well in these cases. Diffraction from dielectric edges constitutes one important exception, since Xpatch does not incorporate an accurate mechanism to account for this phenomenon. This produces errors in the backscatter response at oblique incidence angles (both in azimuth and elevation). These errors are small when only one incidence direction deviates from the normal to the wall, but can become relatively large for oblique incidence in both azimuth and elevation. Although a STTW radar should normally be directed perpendicular to a side of the building, we need to understand the issues related to oblique incidence angles, which are very important in a wide-angle SAR imaging scenario. With regards to FDTD, we noticed some phase errors in the range profiles, which were produced by numerical dispersion. This underscores the importance of following the 10 samples per wavelength rule at the highest frequency in the spectrum. Since we did not meet that criterion for propagation inside the wall materials, we noticed some phase lag in the FDTD-computed late-time peaks, as compared to the Xpatch solution. Another remark was that FDTD generally

produces a higher numerical noise floor than Xpatch, and that could be an issue if we try to model a radar system that requires a very large dynamic range.

In a follow-up to this report, we will investigate SAR images of rooms and buildings, based on computer simulated data. Again, we will use both modeling methods (FDTD and Xpatch) and compare the accuracy of the two. The wide-angle integration mechanism present in a SAR image allows the target localization in cross-range, as well as significant clutter reduction. We will also investigate the trade-offs between certain radar parameters, as well as multipath propagation and scattering issues specific to a STTW scenario.

# References

1. Nag, S.; Barnes, M. A.; Payment, T.; Holladay, G. An ultra-wide band through-wall radar for detecting the motion of people in real time. *SPIE AeroSense Conference Proceedings*, Orlando, FL, April 2002.

2. Yang, Y.; Fathy, A. E. See-through-wall imaging using ultra wideband short-pulse radar system. *2005 IEEE Antennas and Propagation International Symposium*. Washington, DC, pp 334–337 (3B), July 2005.

3. Burchett, H. Advances in through wall radar for search, rescue and security applications. *The Institution of Engineering and Technology Conference on Crime and Security*. London, England, 511–525, June 2006.

4. Dogaru, T.; Nguyen, L.; Le, C. *Computer Models of the Human Body Signature For Sensing Through the Wall Radar Applications*; ARL-TR-4290; U.S. Army Research Laboratory: Adelphi, MD, September 2007.

5. Seidel, S. Y.; Rappaport, T. S. Site-specific propagation prediction for wireless in-building personal communication system design. *IEEE Transactions on Vehicular Technology* **November 1994**, *43*, 879–891.

6. Yang ,C.; Wu, B.; Ko, C. A ray-tracing method for modeling indoor wave propagation and penetration. *IEEE Transactions on Antennas and Propagation* **June 1998**, *46*, 907–919.

7. Tarng, J. H.; Chang, W. R.; Hsu, B. J. Three-dimensional modeling of 900-MHz and 2.44-GHz radio propagation in corridors. *IEEE Transactions on Vehicular Technology* **May 1997**, *46*, 519–527.

8. Yan, Z.; Yang, H.; Parini, C. Two novel FDTD based UWB indoor propagation models. *2005 IEEE International Conference on Ultra-Wideband*. Zurich, Switzerland, pp 124–129, September 2005.

9. Laner, A.; Bahr, A.; Wolff, I. FDTD simulations of indoor propagation. *1994 IEEE Vehicular Technology Conference*. Stockholm, Sweden, pp 883–886 (2), June 1994.

10. Remley, K. A.; Weisshaar, A.; Anderson, H. R. A comparative study of ray tracing and FDTD for indoor propagation modeling. *1998 IEEE Vehicular Technology Conference*, Ottawa, Canada, pp 865–869 (2), May 1998.

11. Talbi, L. Simulation of indoor UHF propagation using numerical technique. *2001 Canadian Conference on Electrical and Computer Engineering*, Toronto, Canada, pp 13–16 (2), May 2001.

12. Wang, Y.; Safavi-Naeini, S.; Chaudhuri, S. K. A hybrid technique based on combining ray tracing and FDTD methods for site-specific modeling of indoor radio wave propagation. *IEEE Transactions on Antennas and Propagation* **May 2000**, *48*, 743–754.

13. Reynaud, M.; Guiffaut, C.; Reineix, A.; Vauzolle, R. Modeling indoor propagation using an indirect hybrid method combining the UTD and the FDTD methods. *$7^{th}$ European Conference on Wireless Technology*, Amsterdam, Netherlands, pp 345–348, 2004.

14. De Oliveira, R.M.S.; Dos Santos, R. O.; Sobrinho, C.L.S.S. Electromagnetic scattering analysis in indoor and outdoor environments by applying FDTD method. *Proceedings of the 2003 Microwave and Optoelectronics Conference*, Iguazu Falls, Brazil, pp 20–23 (1), September 2003.

15. Chama, W. *EM Modelling of a Realistic Room for Through-the-Wall Radar Applications*; Technical Memorandum TM 2007-022; Defence Research and Development Canada: Ottawa, Canada, January 2007.

16. Dogaru, T.; Le, C. *Xpatch and Finite-Difference Time-Domain Modeling of the M1 Tank Radar Signature in the L-band*; ARL-TR-4291; U.S. Army Research Laboratory: Adelphi, MD, September 2007.

17. Taflove, A.; Hagness, S. C. *Computational Electrodynamics: The Finite-Difference Time-Domain*, Artech House, Boston, MA, 2000.

18. Kunz, K.; Luebbers, R. *The Finite-Difference Time-Domain Method for Electromagnetics*, CRC Press, Boca Raton, FL, 1993.

19. *XPATCH User's Manual*, SAIC/DEMACO, Champaign, IL. (This document is export controlled, available to U.S. Government users and DoD Contractors only).

20. Knott, E.; Shaeffer, J.; Tuley, M. *Radar Cross Section*, Artech House, Boston, MA, 1993.

21. ARL MSRC Web page. http://www.arl.hpc.mil (accessed August 2007).

22. Pena, D.; Feick, R.; Hristov, H.; Groto, W. Measurement and modeling of propagation losses in brick and concrete walls for the 900-MHz band. *IEEE Transactions on Antennas and Propagation* **January 2003**, *51*, 31–39.

23. Muqaibel, A.; Safaai-Jazi, A.; Bayram, A.; Attiya, A.; Riad, S. Ultra-wideband through-the-wall propagation. IEE Proceedings – Microwave, Antennas and Propagation, **December 2005**, *152*, 581–588.

24. Stone, W. *Electromagnetic Signal Attenuation in Construction Materials*; NISTIR 6055; National Institute of Standards and Technology: Gaithersburg, MD, October 1997.

25. Yang, C. F.; Ko, C. J.; Wu, B. C.  A free space approach for extracting the equivalent dielectric constants of the walls in buildings.  *1996 IEEE Antennas and Propagation International Symposium*, Baltimore, MD, 1036–1039, July 1996.

26. 3D CAD Browser Web page.  http://3dcadbrowser.com (accessed July 2005).

27. Oppenheim, A. V.; Schafer, R. W.  *Discrete-Time Signal Processing*, Prentice Hall, Englewood Cliffs, NJ, 1989.

28. Shaeffer, J. F.; Hom, K. W.; Baucke, R. C.; Cooper, B. A.; Talcott, N. A.  *Bistatic k-space imaging for electromagnetic prediction codes for scattering and antennas*;  Technical Paper NASA-TP-3569; National Aeronautics and Space Administration:  Langley, VA, July 1996.

29. Balanis, C.  *Advanced Engineering Electromagnetics*, Wiley, New York, 1989.

30. Ruch, G.; Barrick, D. E.; Stuart, W. D.; Krichbaum, C. K.  *Radar Cross Section Handbook*, Plenum Press, New York, 1970.

# Acronyms

ARL         U.S. Army Research Laboratory

CEM        computational electromagnetics

CERDEC   Communications-Electronics Research Development and Engineering Center

CPU        central processing unit

DoD        Department of Defense

FDTD      Finite Difference Time Domain

FFT         Fast Fourier Transform

GTD        geometric theory of diffraction

GUI         graphic user interface

H-H        horizontal-horizontal

HPC        High-Performance Computing

I2WD      Intelligence and Information Warfare Directorate

MSRC     Major Shared Resource Center

PEC        perfect electric conductor

PO          physical optics

SAIC        Science Applications International Corporation

SAR        synthetic aperture radar

STTW      sensing through the wall

UWB        ultra-wideband

V-H         vertical-horizontal

V-V         vertical-vertical

# Distribution List

INTENTIONALLY LEFT BLANK.